Geologic Controls on Permeability Revealed by Borehole Imaging: Case Studies from Sumatra, Indonesia and the Taupō Volcanic Zone, New Zealand

I.C. Wallis[1], D.E. Dempsey[2], and J.V. Rowland[3]

[1] Cubic Earth Ltd., New Zealand

[2] Department of Civil and Natural Resource Engineering, University of Canterbury, New Zealand

[3] School of Environment, University of Auckland, New Zealand

irene@cubicearth.nz

Keywords: *Microresistivity borehole image, acoustic borehole image, feedzone, permeability*

ABSTRACT

We use borehole images, which provide a continuous, high-resolution record of the borehole wall, to evaluate wellbore-scale geologic controls on permeability. Typically, borehole imaging studies include one or more wells from a single reservoir. Ours is unique for its cross-comparative nature, with seven case study wells from four volcanic-hosted geothermal reservoirs, of which two are in Sumatra, Indonesia, and two are in the Taupō Volcanic Zone, New Zealand.

A quantitative well capacity (injectivity index) is included for each case study, which is also novel for a borehole image study. This enabled a key insight: wells with the largest capacity have fracture frequencies that are two to three times greater than lower capacity wells. As well as the influence of fracture frequency, our results reveal the impact of host rock properties and fracture arrangement, hydrothermal alteration, and stress rotation. We introduce a novel category of drilling induced damage that correlates with the distribution of feedzones.

1. INTRODUCTION

Borehole images are a continuous, high-resolution record of the borehole wall. Their acquisition is becoming commonplace in conventional geothermal, with numerous published studies that investigate one or more imaged wells from a geothermal reservoir (e.g., Sone et al., 2023; McNamara et al. 2019; Schoenball and Davatzes, 2017; Masri et al., 2015; McNamara et al., 2015; Halwa et al., 2013; Wallis et al., 2012b; Davatzes and Hickman, 2010; Nemčok et al., 2006; Pramono, 2001; Sudarman et al. 2000; Barton et al., 1998 and more). Subsequently, there is a growing body of knowledge around interpretation of borehole images acquired in geothermal wells, as is reflected by Davatzes and Hickman (2010) and Massiot et al. (2015). Our work highlights that interpretation of borehole images acquired in conventional geothermal must account for thermal stresses on the borehole wall, the mechanical and textural complexity of volcanic and metamorphic rocks, and the impact of hydrothermal alteration on rock properties and log responses. We also introduce a new category of drilling induced tensile fracture that commonly correlates with feedzones

There are two types of borehole images: microresistivity borehole images (MBI) and acoustic borehole images (ABI). MBI and ABI resolve the borehole wall differently and choosing a tool type depends on the program goals. Cost is also a consideration, where some ABI tools can be deployed for a much lower cost than MBI.

MBI were selected for this study because they clearly resolve rock textures. This enables us to consider the influence lithology has on permeability and to better discriminate between tectonic fractures and those lithologic features that are parted at the borehole wall by thermally enhanced hoop stresses (e.g., parting on dike margin, Figure 1 right). ABI may detect lithological variation where that variation is accompanied by changes in elastic rock properties or surface roughness, but not at the same resolution as MBI. Because ABI data includes a wave travel time, and these data enable positive identification of discontinuities that have a large opening aperture at the borehole wall (e.g., Figure 1 left). Neither ABI nor MBI reliably discriminates between water and clay filled fractures with a narrow aperture. Where rock has a layered texture with contrasting resistivities, as can be the case in a foliated metamorphic rock, ABI are preferred for identifying tectonic fractures. However, characterizing bedding dip enables identification of folds and drag bedding. An MBI tool makes contact with the borehole wall and an ABI tool depends on wave return to a centralized receiver. Subsequently, MBI are more likely to successfully characterize oversized, rugose boreholes than ABI, provided the borehole wall is closer than the maximum MBI arm length. Because an ABI generates a 360° image and MBI has gaps between pads, ABI better characterizes drilling induced damage. Acquiring both ABI and MBI and interpreting them together provides the most complete picture of the subsurface environment.

Herein we describe our analysis of borehole image logs from seven wells that were completed into four reservoirs, of which two are in Sumatra, Indonesia and two are in the Taupō Volcanic Zone (TVZ), New Zealand. All borehole images are MBI, with Halliburton's X-tended Range Micro Imager (XMRI) used in Sumatra and Schlumberger's Formation Micro-Imager (FMI) used in New Zealand (Figure 2). Previous studies that used MBI from the case study reservoirs include: Rantau Dedap (RD; Sidik et al., 2016), Muara Laboh (ML; Baroek et al., 2018; Mussofan et al., 2019), Ngatamariki (NM; Dempsey et al. 2013; Halwa et al., 2013; Wallis et al., 2012a), and Wairakei (WK; Massiot et al., 2017; McNamara et al., 2016a; McNamara et al., 2019, Milicich et al., 2020). These studies describe logging operations (Wallis et al., 2012a) or MBI interpretation (Baroek et al., 2018; Halwa et al., 2013; Milicich et al., 2020). They use MBI to inform a local or regional structural model (Mussofan et al., 2019; Sidik et al., 2016; McNamara et al., 2016a; McNamara et al., 2019), or they apply MBI to understanding fluid flux at the wellbore- (Dempsey et al. 2013; Massiot et al., 2017) or reservoir-scale (McNamara et al., 2016a).

Our study differs from previous work by making a broad comparison that includes seven MBI logs from four

ISSN 2703-4275

reservoirs. These case studies are from similar system types (i.e., high-enthalpy, conventional geothermal systems) with commonalities in their volcanic, intrusive, and sedimentary rock. However, they encompass different tectonic histories: TVZ case studies are logs from Quaternary-aged rock that were deposited under consistent tectonic conditions while the GSF case studies include Miocene-aged rock that has experienced a long history of inversion tectonics. The case studies also span a wide range of injectivity, from 3 to >500 t/hr/bar.

In this paper, we describe the methodology used to interpret MBI and how we compare these data to feedzones. Our methodology includes description of a novel category for drilling induced tensile fractures and examples of hydrothermal alteration in and around fractures. We describe the results of comparing MBI data to feedzones. Well names are anonymised. We discuss our results within the context of other similar studies in volcanic and deep circulation geothermal systems.

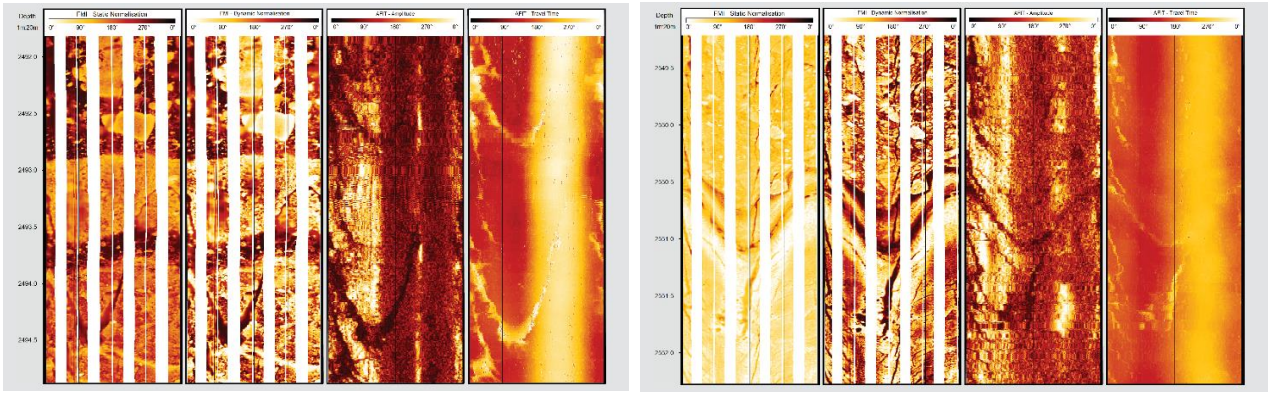

Figure 1: Two cases comparing MBI (FMI-type tool) and ABI (AFIT-type tool) that illustrates how MBI better resolves textures and ABI better resolves those larger aperture features that are open at the wellbore wall. Note that the well is significantly over-sized, so the ABI tool is off center and has minor data loss at the 180 – 360° azimuth range.

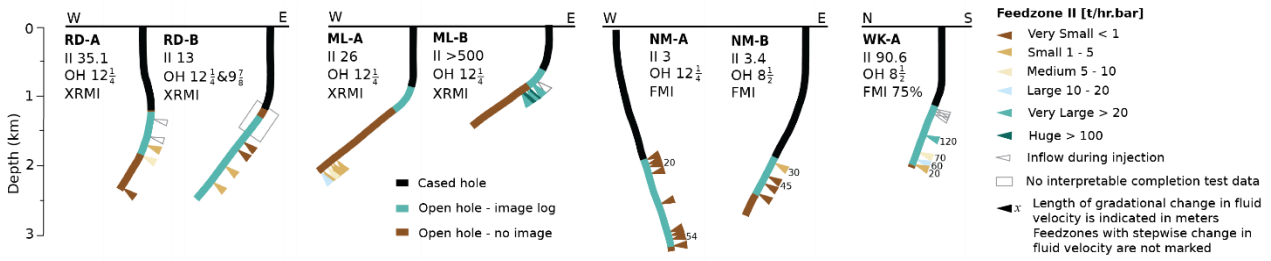

Figure 2: Case study wells. Well capacity as injectivity index (II, t/hr/bar) and open hole diameter (OH, inches). Total injectivity index includes estimated capacity of inflows. MBI types are Schlumberger Fullbore Formation Microimager (FMI) and Halliburton X-tended Range Micro Imager (XRMI). Figure adapted from Wallis et al. (2020).

2. METHODS

To determine wellbore-scale controls on permeability, we compare the geologic features resolved by MBI with the distribution of fluid flux constrained by well completion testing.

2.1 MBI Interpretation

The fundamental approach to borehole image interpretation is well described by Davatzes and Hickman (2010) and Massiot et al. (2015). In this section, we describe those aspects of our interpretation approach that are not covered by these previous works. This includes fracture aperture and mineral fill quantification, a new category of drilling induced tensile factures, and the visual representation of geometric sample bias.

We quantify relative apparent aperture of fractures because larger fractures are more likely to influence borehole hydrology. We define apparent aperture as the measurable thickness on the borehole image, corrected for wellbore deviation. The Luthi and Souhatié (1990) 'excess resistivity' approach to modelling fracture aperture is not used because it was developed using fractures and rock types whose characteristics do not match geothermal conditions (refer to Wallis et al., 2023 for further discussion).

There are two reasons why the apparent aperture is not the actual reservoir aperture. First, MBI tools have an ~0.5-inch depth of penetration into the borehole wall. Consequently, features that are perpendicular to the borehole may appear thinner than those at more acute angles. Second, thermally enhanced hoop stresses may open features that are not open in the reservoir (e.g., Figure 1 right) or simply increase the apparent aperture. Regardless, there is likely to be some gross, scaling relationship between apparent aperture and actual aperture in the reservoir. Given this, we report apparent aperture as six categories that range from very small (< 2 mm) to very large (> 20 mm).

Characterization of mineral fills with MBI remains in its infancy. The standard approach is to classify fractures as electrically conductive (i.e., filled with a conductive mineral like clay or with water) or electrically resistive (i.e., filled with a resistive mineral like quartz or calcite; Davatzes and Hickman, 2010). Bright halos around fractures have previously been recognized (e.g., Halwa et al., 2013). We

ISSN 2703-4275

observed a range of MBI log responses to mineralized fractures in the case study wells (Figure 3).

Our study includes ~5.8 km of MBI image. Because of the large volume of data, our detailed (sub-meter scale) feature-by-feature interpretation quantifies only non-haloed conductive fractures (NHC-fractures) and drilling induced damage because they are most likely to enable characterisation of the controls on permeability. The lithologic context revealed by the MBI texture and various kinds of filled fractures were noted and described by zone. There is substantial scope to build on this work through the analysis of filled fractures and lithologic features, especially within the context of detailed cuttings/core analysis.

We propose a new category of drilling induced tensile fractures (DITF) and refer to them as 'interacting DITF'. They are tensile cracks that tend to form on or between other discontinuities, common NHC-fractures (Figure 4). They occur at a wider range of azimuths and tilts than the borehole axial and en echelon DITF. The intensity of interacting DITF can be so great that the borehole wall appears to be coming apart like a jigsaw (e.g., Figure 4 right), so they may contribute to borehole oversizing. Wide aperture interacting DITF are common around zones with multiple very large, apparently open tectonic fractures (e.g., Figure 4 left).

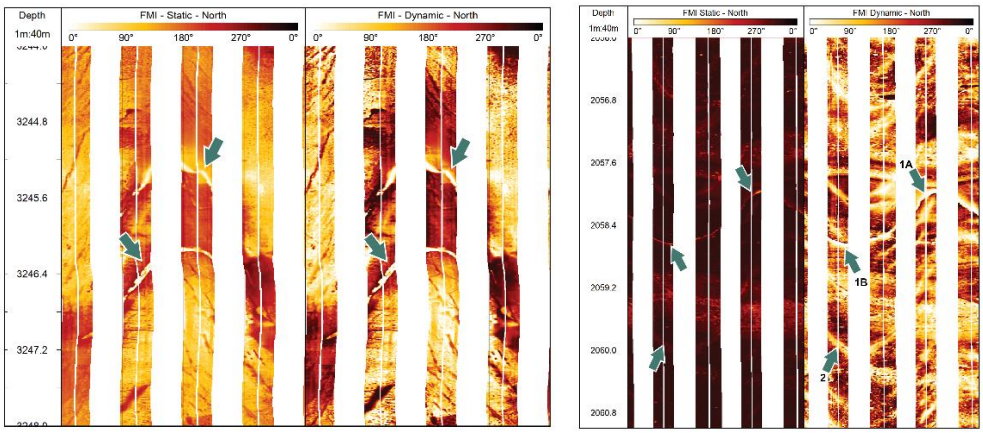

Figure 3: Examples of fracture alteration resolved by MBI. Left: arrows indicate fractures filled with a resistive mineral and surrounded by a relativity conductive alteration halo. Right: 1A/B indicates a bright halo on a fracture's apices that is likely due to current buildup as the tool passes a closed fracture. 2 indicates bright halo along the length of a conductive fracture that is likely due to current attracted to a very conductive mineral (e.g., pyrite).

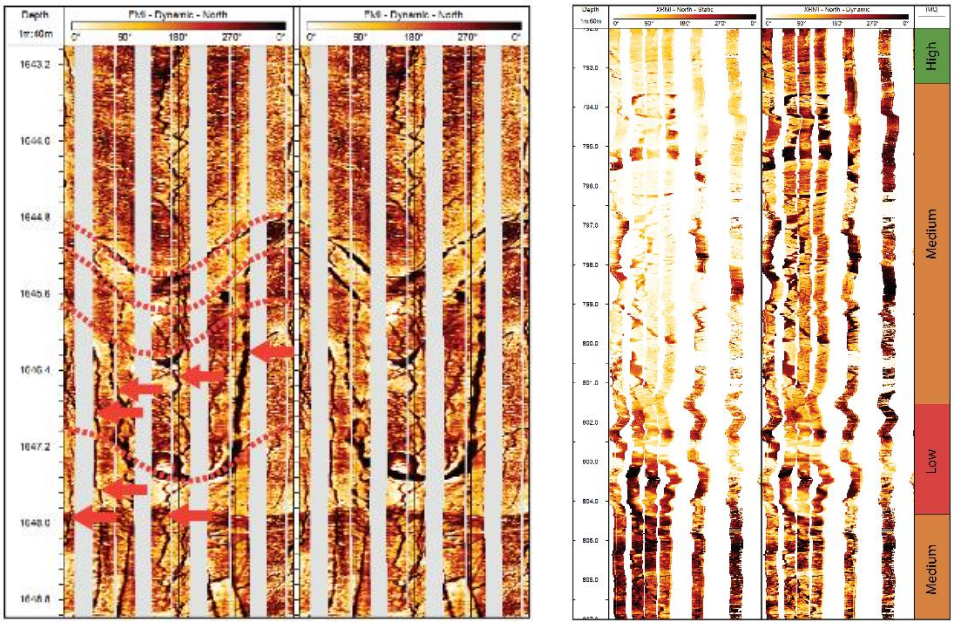

Figure 4: Two examples of interacting DITF. Left: interacting DITF (arrows) form between likely open fractures (dashed lines). Right: intense interacting DITF intersecting fractures likely play a role in borehole oversizing and poor image quality.

We must consider geometric sample bias when relating features identified in a borehole image to the reservoir. Seminal work by Terzaghi (1965) reveals how geometric sample bias operates when a three-dimensional fracture network is sampled along a line (outcrop scanline or well path). Fractures perpendicular to the well path are most likely to be intersected while those parallel to the well path are least likely to be intersected. Terzaghi (1965) identified that fractures < 17.5° to the borehole are very rarely sampled and she coined the term 'blind zone' for this persistent gap in data

ISSN 2703-4275

(Figure 5). The Terzaghi correction is an approach that applies a weighting to each fracture based on the angle it forms with the wellbore. We do not use the Terzaghi correction because it does not compensate for the effect of the blind zone on the data distribution and may generate distortion.

All stereonets in this study include blind zone contours for the average well path within the logged interval (Fractoolbox, 2023; Wallis et al., 2020). Examples from Fish Lake Geothermal System, USA illustrates how major changes in wellbore geometry within the logged interval will appreciably impact the location of the blind zone (Wallis et al., 2023). However, the logged interval of the case studies herein is sufficiently consistent that average isogenic contours reasonably represent geometric sample bias.

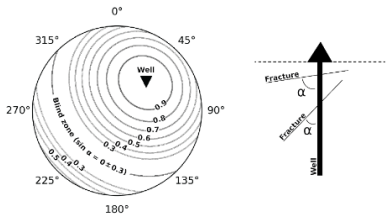

Figure 5: Lower hemisphere, Schmidt stereonet with isogenic contours that map the degree of geometric sample bias for a well inclined 45° to the NE. Figure adapted from Wallis et al. (2020a).

2.3 Permeability Distribution and Magnitude

We use injectivity index (II) as the indicator of permeability because these data were (A) available for all case studies and (B) acquired around the same time as the MBI, where the latter avoids complexity related to permeability improvement or damage. Well capacity and feedzone distribution interpretations were made by company reservoir engineers (Rudy Martikno, Supreme Energy; George Allan, Mercury Energy; Katie McLean, Contact Energy). Feedzones were identified using joint interpretation of pressure (P), temperature (T) and spinner (S) data acquired under injection and PT acquired in static conditions as the well heats (Zarrouk and McLean, 2019). We use the verbal categories in Tables 1 and 2 to discuss wells and feedzone permeability.

Even without operational issues, such as tool or pump calibration faults, completion test data may not accurately reflect the feedzone distribution. The perforated liner, which is typically installed prior to completion testing, will partially obscure feedzones. By comparing PTS logs acquired prior to and after the perforated liner is installed, Goble and McLean (2020) established that the perforated liner made feedzones appear wider and shallower, and merged small discrete feedzones into a single zone. On average, feedzones were shifted 17 m shallower after the liner was installed and feedzone widths were doubled. Goble and McLean (2020) also found some cases where minor feedzones were present in one of the injection tests but not the other. Their study also found that test flow rate influenced the apparent depth of the feedzone, such that they appear 1 – 5 m shallower at lower flow rates. Given that all seven case studies were tested with a liner installed, correlations up to 20 m from the feedzone are considered.

Feedzones do not have a one-to-one relationship to permeability. Flux through the feedzone is a function of the pressure difference between the well and reservoir, fluid viscosity and density, and the permeability. A feedzone below the pressure pivot point (i.e., the one point on the pressure profile that is tied to reservoir pressure) will appear larger during injection than it would during production. The reverse is true for a feedzone above the pivot point.

In low or very-low permeability wells, high resolution analysis of static temperature may be used to identify hydraulically conductive fractures. Low-rate flux into or out of the well under these conditions generates a local temperature change (ΔT) that can be correlated to the imaged fracture distribution. This approach was successfully applied by Barton et al. (1995), who pioneered evaluating the likelihood that borehole imaged discontinuities are hydraulically conductive using slip tendency modelling. However, this fine-scale correlation between static temperature and MBI is not appropriate in a conventional geothermal well with moderate permeability or above. Even when not producing, these wells may have complex internal flow dynamics, such as interzonal flows and internal borehole convection. Feedzones identified under injection are more substantial than the inflections resolved by temperature logging of very low permeability wells. A conventional geothermal well can contain many fractures that, while hydraulically conductive, are not sufficiently permeable or connected to generate a feedzone that can be detected with completion testing.

Table 1: Verbal categories that relate injectivity index to a scale of relative permeability.

Permeability category	Well II [II, t/hr/bar]
Very low permeability	< 1
Low permeability	1 – 5
Moderate permeability	5 – 20
Moderately high permeability	20 – 50
High permeability	50 – 100
Very high permeability	> 100

Table 2: Verbal categories for feedzone II, which is a proportion of total II allocated based on relative contribution.

Category	Feedzone II [t/hr/bar]
Very small	< 1
Small	1 – 5
Medium	5 – 10
Large	10 – 20
Very large	> 20
Huge	> 100

3. RESULTS

Plots comparing MBI interpretation to feedzones for three of the seven case studies are included here (Figures 7, 8, and 9) and the remainder can be found in Wallis (2023). Simple average fracture frequencies were calculated for each case study by dividing the number of NHC-fractures by the total length of MBI (**Error! Reference source not found.**). There is a relationship between these simple average frequencies and the total well capacity: WK-A (Figure 6) and ML-B are high to very high permeability wells and have an average fracture frequency that is 2 – 3 times higher than the other case studies (1.89 and 2.15 NHC-fractures/m, respectively and all others are 0.44 – 0.87 NHC-fractures/m).

Comparing the feedzone locations with the MBI revealed that, in all but one case, there was no great difference in the fracture orientation within feedzones when compared with their surrounds. There were, however, three other groups of

ISSN 2703-4275

factors that correlate with the feedzone distribution. We describe these below.

Increased fracture frequency or aperture: Just over a third of feedzones have a distinct peak in fracture frequency while nearly half correlate with fractures classified as Very Large or Huge. Poor image quality due to borehole oversizing or image artifacts also affects just over a third of the feedzones. In ML-B, RD-A, NM-A and WK-A, poor image quality has reduced frequency of at least one feedzone. However, as illustrated by the high fracture frequency and only one small feedzone in the andesite interval of NM-B (Figure 8), an increased fracture frequency may not generate a feedzone. In this case study, it is possible that the numerous low-angle fractures that are poorly oriented for re-shear are not contributing appreciably to fluid flow (Wallis et al., 2020).

Perturbations of the stress field: Just over a third of feedzones coincide with rotations in the average azimuth of borehole axial or en echelon DITF. Three quarters of the feedzones correlate with the presence of interacting DITF. This is most striking in the larger permeability wells, such as WK-A and ML-B, where the borehole wall at feedzones appears to be parting like a jigsaw breccia due to the intense interaction between tensile fractures and NHC-Fractures.

Lithological variation (primary porosity and mechanical controls on fracturing): Of those MBI where quality is sufficiently good to determine the background lithologic textures, nearly half of the feedzones are located where lithology is different in some way from the surrounds. NM-B and RD-B have feedzones that correlate with a poorly to very poorly sorted breccia. WK-A shallow feedzones are coincident with a highly heterogeneous stack of alternating massive and brecciated rhyolite lava. As well as the potential for primary porosity, it is possible that this heterogeneity plays a role in generating a complex, connected permeability network. Although image quality is too poor to discern the detail of lithologic texture, the feedzone imaged in ML-B is hosted in an interval with higher average resistivity that indicates a different local lithology or, perhaps, less clay alteration.

These case studies also shed light on what conditions not conducive for feedzone-scale permeability. Two case studies have long intervals that are devoid of NHC-Fractures and feedzones. NM-B (Figure 8) has many fractures from in the top 255 m of the log (2,045 – 2,300 m-MDRF), but they are mineralized (i.e., resistive fractures or conductive fractures with a halo). The feedzone in this depth interval is coincident with the small cluster of NHC-Fractures and an apparent stress rotation, and perhaps both the result of recently active faulting. This case lends further support to the hypothesis that, without re-rupture, fractures in a geothermal system may become incapable of hosting feedzone-scale fluid flow as they are plugged by hydrothermal alteration.

The upper 522 m (1,248 – 1,770 m-MDRF, Figure 7) of RD-B is virtually devoid of fractures, either NHC-fractures or those with signatures of mineral fills. This interval includes three lithologies: subaqueous debris flow, rhyolite tuff, and dacite tuff. Average resistivity in this interval is conductive compared to the rest of the well, perhaps indicating the presence of clay minerals. If a greater proportion of clay alteration is present, then perhaps this has reduced the likelihood for brittle failure that creates permeable fractures. Tensile fractures are nearly absent to down to 1,704 m-MDRF (top 456 m), which is 4 m below the top of the rhyolite tuff. This indicates that there has been a change in tensile rock strength with the change in primary lithology. RD-A has a 461 m interval of subaqueous debris flow and dacite tuff that are relatively conductive when compared with the rest of the MBI (1,269 – 1,730 m-MDRF). In contrast with RD-B, the conductive interval in RD-A contains numerous NHC-Fractures and tensile fractures. Future work that investigates the mineralogical difference between these two relatively conductive zones may shed light on this contrast.

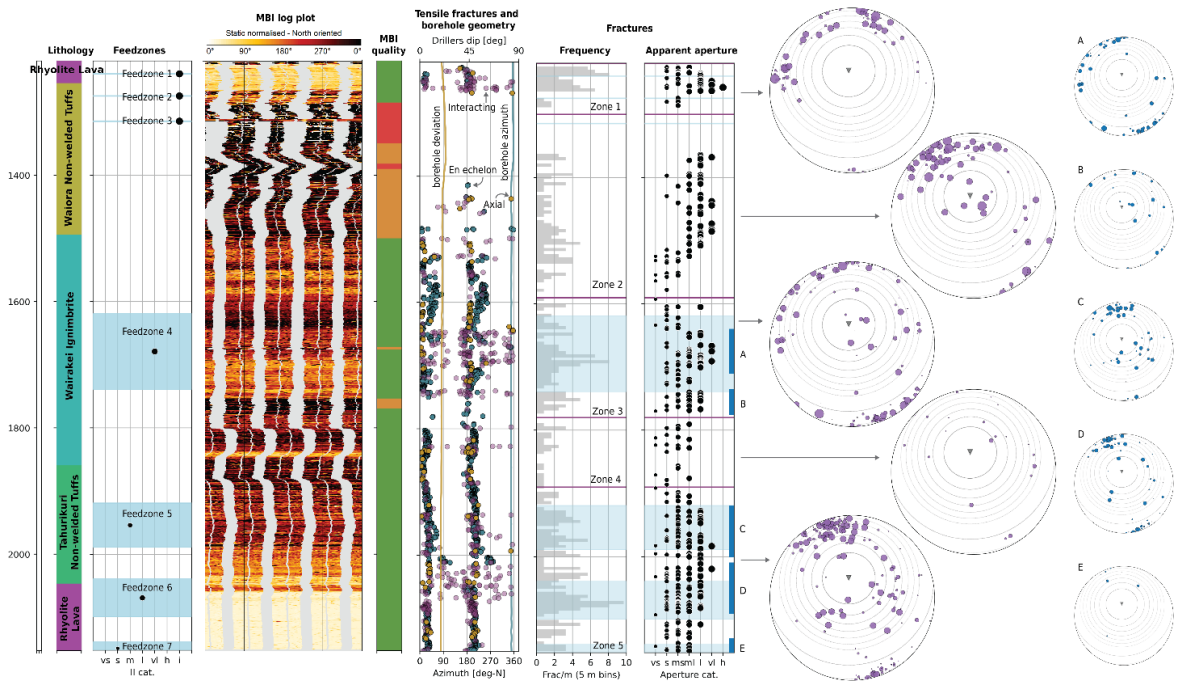

Figure 6: WK-A MBI interpretation results with the provided feedzones and stratigraphy. Light blue bars reflect feedzone thickness and dark blue bars labelled A – E related to the stereonets on the far right.

ISSN 2703-4275

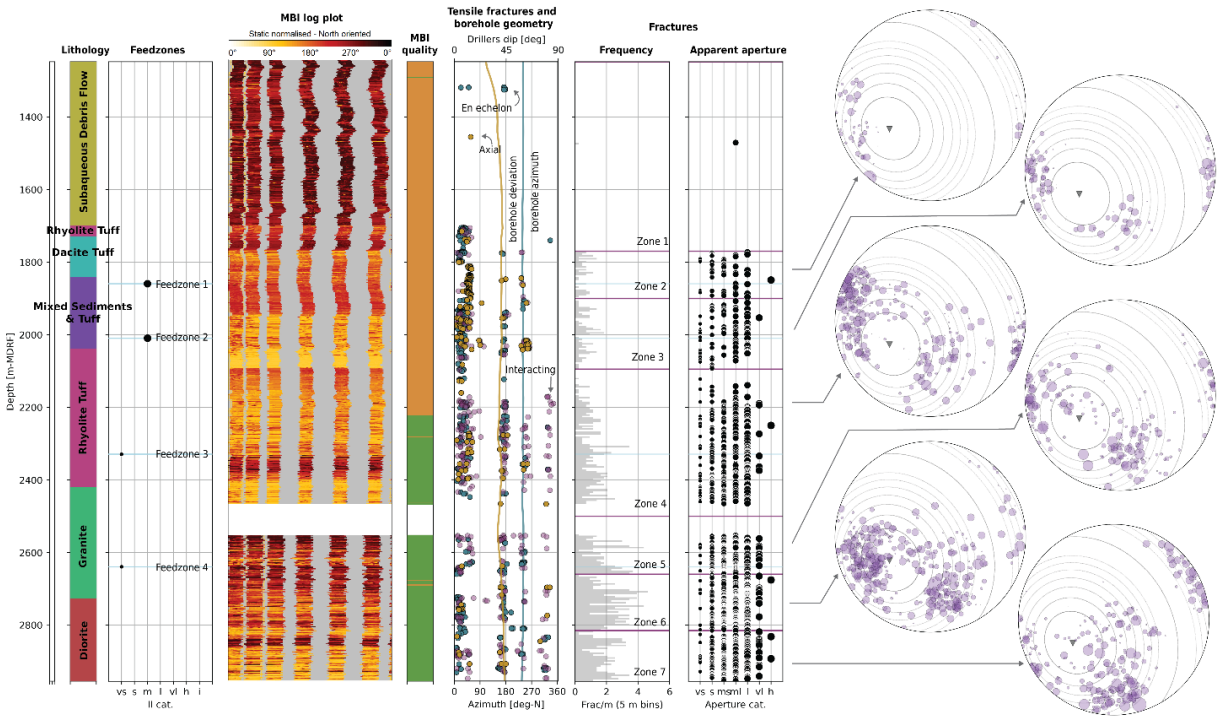

Figure 7: RD-B MBI interpretation results with the provided feedzones and stratigraphy.

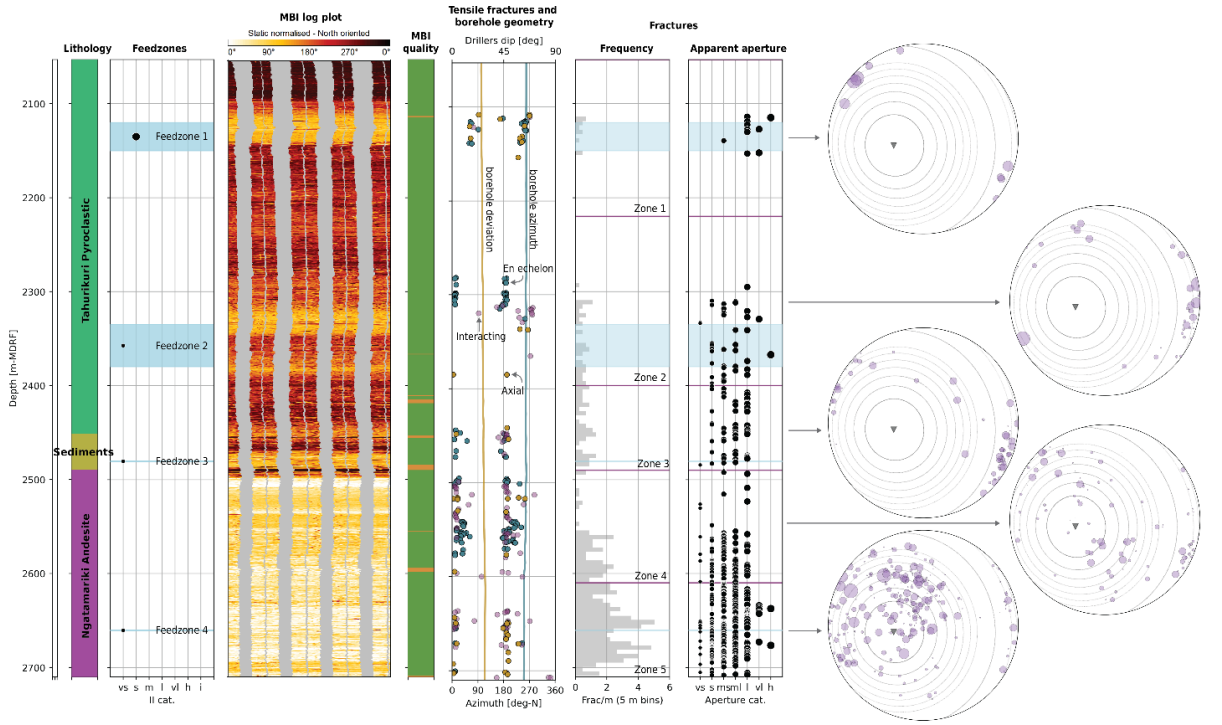

Figure 8: NM-B MBI interpretation results with the provided feedzones and stratigraphy.

4. DISCUSSION

There are a number of other studies that evaluate one or more image logs acquired in volcanic or deep circulation systems. Most found patterns like those described in the results above, with two exceptions: (1) ours is the first study to note the relationship between total well injectivity and average fracture frequency, which highlights the value of a broadly comparative study design and the importance of including quantitative well capacity, and (2) the identification of interacting-type tensile fractures and their relationship to feedzones is novel.

NHC-Fracture frequency correlates with total injectivity magnitude, such that those wells with injectivity above the P10 for geothermal wells have 2 – 3 times more NHC-

Fractures per meter than other wells. One case each from the Sumatran and Taupō Volcanic Zone sets fall into this high NHC-Fracture frequency, high injectivity category, which suggests that: (A) this relationship applies to both andesitic arc and magmatic rift terrains, and (B) that large differences in NHC-Fracture frequency track with the magnitude of injectivity even in those systems with a broad, virtually unconstrained thermal anomaly (Wallis et al., 2017). Fracture density within or adjacent to a fault zone can be enhanced by a change in fault geometry, intersection with other faults, or intersection with pre-existing anisotropy such as bedding contacts or igneous layering (Tripp and Vearncombe, 2004). Similar processes may be the mechanism responsible for the very high fracture frequencies observed herein.

Like our study, feedzones have been found to correlate with fracture frequency and/or aperture and, less commonly, variation of lithology in other geothermal systems. Examples within the Taupō Volcanic Zone include Rotokawa Geothermal System (McNamara et al., 2015). Although located in the same setting as Wairakei and Ngatamariki, this reservoir has a geometry that more resembles the Sumatran systems (Sewell et al., 2012; Hernandez et al., 2015; McNamara et al., 2016b). Evaluation of three ABI logs from that resource revealed that all but one feedzone contained wide aperture fractures and around two thirds had peaks in fracture frequency (McNamara et al., 2015). However, analogous to the case studies herein, two thirds of the wide aperture fractures and 60% of the peaks in fracture frequency in the Rotokawa cases had no correlating feedzone. Recently published work that evaluated four image logs at Wairakei found that wide aperture fractures were preferentially located at feedzone depths, high fracture density is located both within and outside of feedzone depths, and that, with a few exceptions, fracture orientations at feedzones were consistent with the overall trend (McNamara et al. 2019). This is generally consistent with our findings for WK-A; although, our results show that there is an interval with wide aperture fractures and no feedzone (Zone 2, Figure 6).

Wayang Windu Geothermal System, Indonesia, is the same system type as the Sumatran cases, except that it has an expansive vapour dominated zone (Bogie et al., 2008; Raharjo et al., 2016). Analysis of 16 borehole image logs at Wayang Windu found that fracture frequency is high at feedzones, generally three times the average (Masri et al., 2015). Fracture frequency also had a lithologic trend, with a higher frequency in andesite lavas than in tuffs and breccias. At Darajat in Indonesia, image logging identified an increase in fracture frequency with depth, which correlated with a shift to more brittle rocks such as andesite lava and, in places, microdiorite (Pramono, 2001). MBI at Karaha–Telaga Bodas, Indonesia found two significant fluid loss zones that were devoid of fractures and were, instead, relatively conductive rock with either conductive or resistive bedding planes (Nemčok et al., 2007). These Indonesian cases highlight the role lithology may have in controlling the distribution of feedzones, as is also indicated by our results.

Amagmatic, deep circulation system cases include San Emidio Geothermal System, USA where the three MBI and one ABI were evaluated against the distribution of drilling fluid losses and feedzones (Sone et al., 2023). This study revealed some of the same trends described above, with wide aperture fractures and localized zones of high fracture frequency appearing to play some controlling role. Interestingly, the depth where fault damage zone architecture was identified in that study did not correlate with any indicators of permeability. The study of six ABI logs at Dixie Valley, USA included no comment on the frequency or apparent aperture of imaged fractures (Barton et al., 1998). However, the study did find that flow zones were located where both imaged fractures and the Dixie Valley Fault Zone were critically stressed and, in some cases, where low-angle fractures were also present.

Our results include numerous intervals with wide aperture fractures and/or peaks in fracture frequency that have no corresponding feedzones. This may be due to the fundamental nature of a feedzone: features imaged at the borehole wall must connect to the wider permeability network to either accept or produce fluids. Alternatively, a proportion of the fractures that appear open at the borehole wall may not be hydraulically meaningful perhaps because they are poorly oriented for reactivation given the stress field, as was indicated by the Dixie Valley results (Barton et al., 1998) and NM-B (Wallis et al., 2020).

Stress tensor rotations are captured in the borehole images by shifts in the azimuth of axial or en echelon DITF. For the three image logs evaluated at Rotokawa, half had associated local stress tensor rotations (McNamara et al., 2015). In their study at Wairakei, McNamara et al. (2019) found tensile fracture rotations in all four wells reviewed and that the frequency of drilling induced damage tracked with the fracture frequency. However, no comment was offered on how this correlated with the distribution of permeability. Prominent stress rotations were found in borehole images acquired at Coso Geothermal System, some found near large fault intersections (Davatzes and Hickman, 2010) and others without clear evidence of a nearby fault (Schoenball and Davatzes, 2017). However, no comment was made in either study on the relationship between these rotations and indicators of fluid flux.

We found that just over a third of feedzones coincide with stress rotations. Local rotations in the stress tensor away from the background trend are most likely to be the residual signal of fault rupture (Zoback 2010, Davatzes and Hickman, 2010). Subsequently, it is likely that feedzones with these rotations exist, in part, due to recent fault rupture, especially cases like FZ1 in NM-B (Figure 8) where the rotation also coincides with the only NHC-Fractures in a ~520 m long interval.

Peaks in the frequency of interacting DITF correlate with around three quarters of the feedzones. They are most frequent and have widest apertures around feedzones of highly permeable wells (WK-A and ML-B). It is possible that these off-axis DITF signal residual stress from recent fault rupture. It is also possible that thermally enhanced tensile hoop stresses may play a role, perhaps through the loss of a large volume of drilling fluid into a small interval of formation. Although the mechanism requires further investigation, the correlation with feedzones is clear.

Finding that the low permeability intervals NM-B is dominated by resistive and haloed conductive fractures lends weight to the hypothesis that, without re-rupture, fractures in a geothermal system may become impermeable over time. Change of fracture permeability with time is recognized elsewhere. For instance, thin section analysis at Muara Laboh identifies late-stage infilling of calcite, quartz and prehnite alteration that is thought to be responsible for local

ISSN 2703-4275

reductions in permeability (Baroek et al., 2018; Mussofan et al., 2018). Noting that quartz and calcite would appear as resistive mineral fills, while prehnite, which is a calcium aluminosilicate, may be more conductive. However, mapping between the distribution of resistive or conductive fractures with haloes may be complex, as is indicated by cases where haloed fractures are found within feedzones (McNamara et al., 2019). Analysis of all MBI fracture types, and their cross-cutting relationships, in partnership with mineralogical paragenesis may provide insight into permeability evolution.

5. CONCLUSION

We presented seven case studies where that compare geologic features resolved by borehole images to well permeability (total injectivity and feedzone locations). Although our case studies are from four different volcanic-hosted geothermal reservoirs that are in two tectonic settings, they yielded similar trends. Our inclusion of quantitative well capacity and use of a cross-comparative study is novel and has enabled us to identify that high and very high permeability wells have an average fracture frequency 2 – 3 times greater than lower permeability wells. Our study revealed that feedzones variously correlate with increased fracture frequency and aperture, perturbations of the stress field, and lithological variation. These findings are similar to previous studies in volcanic and deep circulation geothermal systems. Our observations of mineralized fractures in the borehole images supports the hypothesis that, without re-rupture, fractures may become incapable of hosting feedzone-scale fluid flow as they become plugged by hydrothermal alteration. We introduce a new category of DITF (termed 'interacting' DITF) that strongly correlates with the distribution of permeability, especially in large capacity wells. The mechanism driving the formation of these interacting DITF remains unequivocal and requires further investigation.

ACKNOWLEDGEMENTS

This study is the result of doctoral research, with the first three years funded by a University of Auckland scholarship. The authors thank Supreme Energy, Mercury Energy and Contact Energy for providing data.

REFERENCES

Barton, C. A., Zoback, M. D., & Moos, D. (1995). Fluid flow along potentially active faults in crystalline rock. *Geology*, *23*, 683–686.

Barton, C. A., Hickman, S. H., Morin, R., Zoback, M. D., & Benoit, D. (1998). Reservoir-scale fracture permeability in the Dixie Valley, Nevada, geothermal field. *Proceedings, Workshop on Geothermal Reservoir Engineering. Stanford, California*, 315–322.

Baroek, M., Stimac, J., Sihotang, A. M., Putra, A. P., & Martikno, R. (2018). Formation and fracture characterization of the Muara Laboh Geothermal System, Sumatra, Indonesia. *Geothermal Resources Council Transactions*, *42*.

Bogie, I., Kusumah, Y. I., & Wisnandary, M. C. (2008). Overview of the Wayang Windu geothermal field, West Java, Indonesia. *Geothermics*, *37*(3), 347–365.

Davatzes, N. C., & Hickman, S. H. (2010). Stress, fracture, and fluid-flow analysis using acoustic and electrical image logs in hot fractured granites of the Coso Geothermal Field, California, U.S.A. In C. Pöppelreiter, C. García-Carballido, & M. Kraaijveld (Eds.), *Dipmeter and Borehole Image Log Technology* (pp. 159–293).

Dempsey, D. E., Clearwater, J., Kellar, S., & Wallis, I. C. (2013). Validation of a Coupled Thermal-Hydrological-Mechanical Model Though a Comparative Study of Shear Stimulation in Two Geothermal Environments: USA and New Zealand. *Proceedings, New Zealand Geothermal Workshop.*

Fractoolbox (2023) *https://github.com/ICWallis/fractoolbox*

Goble, I., & McLean, K. (2020). Accurate location of feed zones: Assessing obscuration by the liner in geothermal wells. *Proceedings, New Zealand Geothermal Workshop*.

Halwa, L., Wallis, I. C., & Lozada, G. T. (2013, November 17). Geological analysis of the volcanic subsurface using borehole resistivity images in the Ngatamariki Geothermal Field, *Proceedings, New Zealand Geothermal Workshop*.

Hernandez, D., Addison, S., Sewell, S., Azwar, L., & Barnes, M. (2015). Rotokawa: Reservoir response of 172 MW geothermal operation. Proceedings, *New Zealand Geothermal Workshop.*

Milicich, S. D., Massiot, C., McNamara, D. D., & Sepulveda, F. (2020). Volcanic texture identification and influence on permeability using borehole resistivity image logs in the Taupo Volcanic Zone, New Zealand. *Proceedings, Workshop on Geothermal Reservoir Engineering.* Stanford, California.

Masri, A., Barton, C. A., Hartley, L., & Ramadhan, Y. (2015). Structural permeability assessment using geological structural model integrated with 3D geomechanical study and discrete facture network model in Wayang Windu Geothermal Field, West Java, Indonesia. *Proceedings, Workshop on Geothermal Reservoir Engineering.* Stanford, California.

Massiot, C., McNamara, D. D., & Lewis, B. (2015). Processing and analysis of high temperature geothermal acoustic borehole image logs in the Taupo Volcanic Zone, New Zealand. *Geothermics*, *53*, 190–201.

Massiot, C., McLean, K., McNamara, D., Sepulveda, F., & Milicich, S. D. (2017). Discussion between a reservoir engineer and a geologist: Permeability identification from completion test data and borehole image logs integration. *Proceedings, New Zealand Geothermal Workshop.*

McNamara, D. D., Massiot, C., Lewis, B., & Wallis, I. C. (2015). Heterogeneity of structure and stress in the Rotokawa Geothermal Field, New Zealand. *Journal of Geophysical Research: Solid Earth*, *120*(2), 1243–1262.

McNamara, D., Bannister, S., Villamor, P., Sepulveda, F., Milicich, S. D., Alcaraz, S. A., & Massiot, C. (2016a). Exploring structure and stress from depth to surface in the Wairakei Geothermal Field, New Zealand. *Proceedings, Workshop on Geothermal Reservoir Engineering.* Stanford, California.

McNamara, D. D., Sewell, S., Buscarlet, E., & Wallis, I. C. (2016b). A review of the Rotokawa Geothermal Field, New Zealand. *Geothermics*, *59*, 281–293.

ISSN 2703-4275

McNamara, D. D., Milicich, S. D., Massiot, C., Villamor, P., McLean, K., Sépulveda, F., & Ries, W. F. (2019). Tectonic Controls on Taupo Volcanic Zone Geothermal Expression: Insights from Te Mihi, Wairakei Geothermal Field. *Tectonics*, *38*(8), 3011–3033.

Mussofan, W., Stimac, J. A., Baroek, M., Colvin, A., Sidik, R. P., Ganefianto, N., & Santana, S. (2019). Thick silicic volcanic sequences at Muara Laboh and Rantau Dedap geothermal fields, Sumatra, Indonesia: Implications for reservoir architecture and permeability. *Proceedings, New Zealand Geothermal Workshop.*

Mussofan, W., Baroek, M. C., Stimac, J., Sidik, R. P., Ramadhan, I., & Santana, S. (2018). Geothermal resource exploration along Great Sumatera Fault segments in Muara Laboh: Perspectives from geology and structural play. *Proceedings, Workshop on Geothermal Reservoir Engineering*. Stanford, California.

Nemčok, M., Moore, J. N., Christensen, C., Allis, R., Powell, T., Murray, B., & Nash, G. (2007). Controls on the Karaha–Telaga Bodas geothermal reservoir, Indonesia. *Geothermics*, *36*(1), 9–46.

Pramono, B. (2001). Density and orientation of fractures along the Gagak Fault and feed zones in the Darajat Geothermal Field. *Proceeding of the 5th Inaga Annual Scientific Conference & Exhibitions*, Yogyakarta, Indonesia.

Raharjo, I. B., Allis, R. G., & Chapman, D. S. (2016). Volcano-hosted vapor-dominated geothermal systems in permeability space. *Geothermics*, *62*, 22–32.

Schoenball, M., & Davatzes, N. C. (2017). Quantifying the heterogeneity of the tectonic stress field using borehole data. *Journal of Geophysical Research: Solid Earth*.

Sewell, S., Cumming, W., Azwar, L., & Bardsley, C. (2012). Integrated MT and Natural State Temperature Interpretation for a Conceptual Model Supporting Reservoir Numerical Modelling and Well Targeting at the Rotokawa Geothermal Field, New Zealand. *Proceedings, Workshop on Geothermal Reservoir Engineering*. Stanford, California.

Sidik, R. P., Mussofan, W., Santana, S., & Azis, H. (2016). Structure geology of southwestern sector Rantau Dedap Geothermal Field. *Proceedings Annual 4th Indonesia International Geothermal Convention & Exhibition*, Jakarta, Indonesia.

Sone, H., Mudatsir, O., Jin, Z., Folsom, M., Ramirez, G., & Feigl, K. L. (2023). WHOLESCALE - Characterization of Conductive Fractured Zones Based on Borehole Data at San Emidio Geothermal Field, Nevada. *Proceedings, Workshop on Geothermal Reservoir Engineering.* Stanford, California.

Sudarman, S., Guntur, B., Setiadji, D., & Sumantri, Y. (2000). Mapping reservoir permeability with geoelectrical, FMS and spinner data, Kamojang Field, Indonesia. *Proceedings World Geothermal Congress 2000.*

Terzaghi, R. D. (1965). Sources of error in joint surveys. *Geotechnique*, *15*(3), 287–304.

Tripp, G. I., & Vearncombe, J. R. (2004). Fault/fracture density and mineralization: A contouring method for targeting in gold exploration. *Journal of Structural Geology*, *26*(6–7), 1087–1108.

Wallis, I. C., McCormick, S., Sewell, S., & Boseley, C. (2012a). Formation assessment in geothermal using wireline tools—Application and early results from the Ngatamariki Geothermal Field, New Zealand. *Proceedings, New Zealand Geothermal Workshop*.

Wallis, I. C., McNamara, D., Rowland, J. V., & Massiot, C. (2012b). The nature of fracture permeability in the Basement Greywacke at Kawerau Geothermal Field, New Zealand. *Proceedings, Workshop on Geothermal Reservoir Engineering*. Stanford, California.

Wallis, I. C., Rowland, J. V., Cumming, W., & Dempsey, D. E. (2017). The subsurface geometry of a natural geothermal reservoir. *Proceedings, New Zealand Geothermal Workshop*.

Wallis, I. C., Rowland, J., Dempsey, D., Allan, G., Sidik, R., Martikno, R., McLean, K., Sihotang, M., Azis, H., & Baroek, M., (2020). Approaches to imaging feedzone diversity with case studies from Sumatra, Indonesia and the Taupo Volcanic Zone, New Zealand. *Proceedings, New Zealand Geothermal Workshop.*

Wallis, I.C. (2023) *The Geologic Controls on Geothermal Fluid Flux at the District-, Reservoir-, and Wellbore-Scale.* Unpublished PhD Thesis, University of Auckland.

Wallis, I.C., Milton, A., Brown, Z., Davis, L., Casteel, J., Peters, B. (2023) Faults, fractures, formation and stress at Fish Lake: Controls on wellbore-scale permeability in a deep circulation geothermal system. *Geothermal Resources Council Transactions*, *47*.

Zarrouk, S. J., & McLean, K. (2019). *Geothermal well test analysis: Fundamentals, applications and advanced techniques*. Academic Press, London.

Zoback, M. D. (2010). *Reservoir Geomechanics*. Cambridge University Press.

ISSN 2703-4275